EUROPEAN ORGANIZATION FOR NUCLEAR RESEARCH

CERN-PPE/97-110
11 August 1997

# Measurement of $\eta'(958)$ Formation in Two-Photon Collisions at LEP1

The L3 Collaboration

## Abstract

The formation of the $\eta'$ in the reaction $e^+e^- \to e^+e^-\eta' \to e^+e^-\pi^+\pi^-\gamma$ has been measured by the L3 detector at a centre-of-mass energy of 91 GeV. The radiative width of the $\eta'$ has been found to be $\Gamma_{\gamma\gamma} = 4.17 \pm 0.10$ (stat.) $\pm$ 0.27 (sys.) keV. The $Q^2$ dependence of the $\eta'$ formation cross section has been measured for $Q^2 \leq$ 10 GeV$^2$ and the $\eta'$ electromagnetic transition form factor has been determined. The form factor can be parametrised by a pole form with $\Lambda = 0.900 \pm 0.046$ (stat.) $\pm$ 0.022 (sys.) GeV. It is also consistent with recent non-perturbative QCD calculations.

Submitted to *Phys. Lett.*

# 1 Introduction and formalism

High energy $e^+e^-$ storage rings allow the study of two-photon interactions via the collision of virtual photons: $e^+e^- \to e^+e^-\gamma^*\gamma^*$, $\gamma^*\gamma^* \to X$. An important measurement is the two-photon coupling to a C = +1 resonance R. Here we report on a study of the formation of the $\eta'(958)$ in the two-photon reaction $e^+e^- \to e^+e^-\gamma^*\gamma^*$, $\gamma^*\gamma^* \to \eta'$, $\eta' \to \pi^+\pi^-\gamma$, using data collected with the L3 detector at LEP at centre-of-mass energies $\sqrt{s} \simeq 91$ GeV. This measurement has been performed previously at lower energy $e^+e^-$ colliders [1,2] by using various $\eta'$ decay channels.

The four-momentum transfers of the scattered electrons, $q^2$ and $k^2$, are often so small that the electrons go undetected along the beam direction. The photon with highest virtuality defines the variable $Q^2 = -q^2$. If one of the electrons is detected, the event is said to be *tagged*. The strength of the coupling of a meson to two photons, $\Gamma_{\gamma\gamma}$, and the $Q^2$ dependence of the formation cross section give information on the quark content and on the quark dynamics of the bound state. The cross section for the formation of the $\eta'$ is given by:

$$\sigma(e^+e^- \to e^+e^-\eta') = \int d^5\mathcal{L}_{\gamma\gamma}(\alpha_i) \cdot \sigma(W_{\gamma\gamma}, q^2, k^2) \tag{1}$$

where $d^5\mathcal{L}_{\gamma\gamma}$ is the differential luminosity function giving the flux of virtual photons and $\alpha_i (i = 1, ..., 5)$ are the variables describing the scattered electron and positron. The $Q^2$ dependence of the cross section is expressed by the meson electromagnetic form factor $F(q^2, k^2)$:

$$\sigma(W_{\gamma\gamma}, q^2, k^2) = \frac{1}{4}\sqrt{X} \cdot F^2(q^2, k^2) \cdot \frac{\Gamma_{\eta'} m_{\eta'}}{(W_{\gamma\gamma}^2 - m_{\eta'}^2)^2 + m_{\eta'}^2 \Gamma_{\eta'}^2} \tag{2}$$

where $X = [(q \cdot k)^2 - q^2k^2]$ takes into account the matrix element for the coupling of the pseudoscalar state to two virtual photons. The form factor $F$ is usually parametrised with a pole form[1)]:

$$F^2(q^2, k^2) = \frac{64\pi}{m_{\eta'}^3}\Gamma_{\gamma\gamma}(\eta') \cdot [\frac{1}{1 - q^2/\Lambda^2}]^2 \cdot [\frac{1}{1 - k^2/\Lambda^2}]^2 \ . \tag{3}$$

The parameter $\Lambda$ is related to the size of the meson [3] and must be described by any model of $q\bar{q}$ binding. Combining Eqs. 1-3 leads to a proportionality relation between the measured cross section and the two-photon width $\Gamma_{\gamma\gamma}(\eta')$.

The decay rate of $\eta' \to \rho\gamma$ in the two-photon centre-of-mass frame is:

$$d\Gamma_{\eta' \to \rho\gamma} = \frac{1}{32\pi^2} |\mathcal{M}|^2 \frac{p_\gamma}{m_{\eta'}^2} d\Omega \ . \tag{4}$$

Since the $\eta'$ is a spin 0 particle, the transition $0^- \to 1^- + 1^-$ requires that in the $\rho$ rest frame the decay amplitude is:

$$\mathcal{M} = BW(\rho) \cdot \sqrt{2} m_{12} p_1^* p_\gamma^* \sin\theta_1^* \tag{5}$$

where $m_{12}$ is the mass of the $\pi^+\pi^-$ system, $p_\gamma^*$ is the photon momentum, $p_1^*$ is the $\pi^+$ momentum and $\theta_1^*$ is the angle between the $\pi^+$ and the photon direction. Recently it has been claimed [4–6] that a pure $\rho$ Breit-Wigner term is not sufficient to describe the data. A non-resonant

[1)] We follow the form factor definition of Ref. [2,3]. A factor $1/(4\pi\alpha)^2$ would be added to follow the definition of Ref. [17–19] contribution in the $\eta' \to \pi^+\pi^-\gamma$ decay, associated with a possible contribution of the box anomaly, has been included by adding a second term to the $\rho$ Breit-Wigner amplitude:

$$BW(\rho) = \frac{1}{(m_{12}^2 - m_\rho^2) - i m_{12}\Gamma_\rho} + \frac{\xi}{m_{\eta'}^2} exp(i\phi) \tag{6}$$

where $\xi$ is the relative amplitude with phase angle $\phi$. For the $\rho$ mass dependent width $\Gamma_\rho$, the formula of Ref. [7] is used:

$$\Gamma_\rho = \Gamma_0 \left(\frac{p_1^*}{p_0}\right)^3 \frac{m_\rho}{m_{12}} \tag{7}$$

where $p_0 = \sqrt{m_\rho^2 - 4m_\pi^2}/2$ and $\Gamma_0 = 151.2$ MeV is the nominal width of the $\rho$ [8].

The EGPC Monte Carlo generator [9] is used to generate the events. The events $e^+e^- \to e^+e^-R$ ($R = \eta'$, $a_2$) are generated according to the luminosity function of Budnev et al. [10]. The Breit-Wigner shape, the form factor and the decay of the system R are then implemented as described by Eqs. 2-7. The resonance parameters are taken from Ref. [8], except for the value of $\Gamma_{\gamma\gamma}(\eta')$ which is set nominally to 1 keV. The Monte Carlo events were simulated in the L3 detector using the GEANT [11] and GEISHA [12] programs and passed through the same reconstruction program as the data.

# 2 Data analysis

## 2.1 Event selection

The L3 detector [13] has the capability to measure charged particles and photons of low momentum. A trigger, which requires at least two charged particles, each with $p_t > 150$ MeV, back-to-back in the transverse plane within 41°, has a high efficiency for two-photon collision events. For tagged events the trigger demands at least 30 GeV deposited in the small angle electromagnetic calorimeter ($0.9976 \leq |\cos\theta| \leq 0.9997$), in coincidence with at least one track in the central part of the detector.

The candidate $e^+e^- \to e^+e^-\pi^+\pi^-\gamma$ events are selected by requiring:

- *Two oppositely charged tracks.* A track is accepted if it has at least 20 hits out of a maximum of 62 in the central detector ($|\cos\theta| \leq 0.9$) and if its transverse momentum $p_t$ is greater than 130 MeV. To eliminate the lepton channels $e^+e^- \to e^+e^-l^+l^-$ where $l = e, \mu$, the total transverse momentum squared of the two charged tracks $|\vec{p}_t(\pi^+\pi^-)|^2$ must be greater than 0.001 GeV$^2$, as illustrated in Fig. 1a.

- *One photon only.* A cluster in the BGO electromagnetic calorimeter is identified as a photon if it has an energy greater than 140 MeV and it is separated by an angle greater than 10° from both tracks. The angular coverage of the electromagnetic calorimeter is $|\cos\theta| \leq 0.71$ (barrel) and $0.82 \leq |\cos\theta| \leq 0.97$ (endcap).

- *The angle* of the $\pi^+$ in the $\rho$ helicity frame must be such that $|\cos\theta_1^*| < 0.94$, as illustrated in Fig. 1b. This cut reduces non-resonant $\pi^+\pi^-\gamma$ background.

The events are classified into three Groups:

Group I: The events produced by quasi-real photons ($Q^2 < 0.01$ GeV$^2$).

Group II: The intermediate range ($0.01 \leq Q^2 \leq 0.9$ GeV$^2$) where the electron goes undetected and the $Q^2$ is measured from the transverse momentum squared of the $\eta'$.

Group III: The singly tagged events where one electron is detected in the small angle electromagnetic calorimeter ($1.5 \leq Q^2 \leq 10.0$ GeV$^2$) with energy greater than 35 GeV. For this Group, the cut $|\vec{p}_t(\mathrm{e}^{\pm}_{tag}\pi^+\pi^-\gamma)|^2 < 0.05$ GeV$^2$ is applied, where $\mathrm{e}^{\pm}_{tag}$ is the detected electron.

## 2.2 Quasi-real photons and $\Gamma_{\gamma\gamma}(\eta')$

For Group-I events the analysis is limited to photons observed in the barrel region and the cut $|\vec{p}_t(\pi^+\pi^-\gamma)|^2 < 0.01$ GeV$^2$ is applied. The reconstructed $\pi^+\pi^-\gamma$ mass spectrum is shown in Fig. 2. A total of 6767 events are selected, where 2786 are in the $\eta'$ region ($0.85 \leq m(\pi^+\pi^-\gamma) \leq$ 1.05 GeV). The $\eta'$ mass, obtained by a Gaussian fit, is $958 \pm 1$ MeV with $\sigma = 24 \pm 1$ MeV. The mass value is in good agreement with the world average value [8] and the width is consistent with the $\pi^+\pi^-\gamma$ mass resolution as estimated by the Monte Carlo. The enhancement around 1250 MeV is due to the tensor meson, $\mathrm{a}_2(1320)$, whose dominant decay mode is: $\mathrm{a}_2 \to \pi^{\mp}\rho^{\pm} \to \pi^{\mp}\pi^{\pm}\pi^0 \to \pi^{\mp}\pi^{\pm}\gamma\gamma$. If one of the two photons is undetected, these events can pass the selection cuts. The $\mathrm{a}_2$ events were simulated according to the parameter values and the helicity amplitudes measured by us and reported in Ref. [14]. The reconstruction efficiency for a photon is 97.7% independent of its energy ($0.14 \leq E_\gamma < 1$ GeV). The trigger efficiency for Group-I $\eta'$ events is $48 \pm 1\%$. In Fig. 3 the angular distribution of the $\pi^+$ in the $\rho$ helicity frame is presented for the events in the $\eta'$ region. It shows the characteristic distribution of Eq. 5.

The two-photon radiative width $\Gamma_{\gamma\gamma}(\eta')$ is determined by fitting the mass spectrum of Fig. 2 with the two Monte Carlo distributions for the $\eta'$ and the $\mathrm{a}_2$, and a third order polynomial for the background. The fit minimises a $\chi^2$ function with expected value in each bin $i$ of:

$$E_i = [\Gamma_{\gamma\gamma}(\eta') \cdot BR] \cdot N_i(\eta') + N_i(\mathrm{a}_2) + B_i \tag{8}$$

where $N_i$ are the Monte Carlo expectations for the $\eta'$ and the $\mathrm{a}_2$, and $BR$ is the $\eta'$ branching ratio into $\pi^+\pi^-\gamma$. The free parameters are $\Gamma_{\gamma\gamma}(\eta') \cdot BR$ (in keV units) and the coefficients of the polynomial background, $B_i$. The product of the $\eta'$ two-photon width times branching ratio thus obtained is:

$$\Gamma_{\gamma\gamma}(\eta') \cdot BR = 1.26 \pm 0.03\ (\text{stat.}) \pm 0.06\ (\text{sys.})\ \text{keV} \qquad \chi^2/dof = 131/121\ (\text{C.L.} = 25\%)\ .$$

The fit results are superimposed on the data in Fig. 2. The $\eta'$ peak contains $2123 \pm 53$ events. The systematic uncertainty for the $\Gamma_{\gamma\gamma}(\eta') \cdot BR$ measurement is 5%. The main uncertainties come from the selection: 4% from the cut in the photon energy, 1% from the cut in $|\vec{p}_t(\pi^+\pi^-\gamma)|^2$, 2% for the trigger efficiency and 1% for the background subtraction. Using $BR = 0.302 \pm 0.013$ [8], we obtain:

$$\Gamma_{\gamma\gamma}(\eta') = 4.17 \pm 0.10\ (\text{stat.}) \pm 0.27\ (\text{sys.})\ \text{keV}$$

where the systematic error includes the error on the branching ratio. This result has smaller statistical and systematic errors than any previous experiment [1,2]. It is comparable in precision to the world average value ($4.34 \pm 0.25$ keV) [8]. It is worth noting that recent relativistic quark models [15], which successfully predict the two-photon coupling of tensor mesons, fail to reproduce the value of the two-photon widths of pseudoscalar states. In the best case, the prediction is typically a factor of two below the measurement.

The good resolution of the detector and the high statistics allow an accurate study of the $\rho$ meson line shape in the $\eta' \to \rho\gamma$ decay. In Fig. 4 the uncorrected $\pi^+\pi^-$ mass spectrum is shown. The $\rho$ line shape, given by Eqs. 6 and 7 with $\xi = 0$, has been studied by generating several Monte Carlo samples with different masses and widths. By comparing the data to the Monte Carlo samples, the minimum of $\chi^2$ ($\chi^2 = 34$ for 32 $dof$, C.L. = 37%) is found for the values

$$m_\rho = 766 \pm 2 \text{ MeV} \qquad\qquad \Gamma_\rho = 150 \pm 5 \text{ MeV}.$$

These results agree with the world average, $m_\rho = 768.5 \pm 0.6$ MeV and $\Gamma_\rho = 150.7 \pm 1.2$ MeV [8]. With the same method, the possibility of a non-resonant $\pi^+\pi^-$ contribution parametrised as in Eq. 6 has been tested by varying the $\xi$ and $\phi$ parameters. The best agreement with the data is for $\xi = 0$. The values obtained by previous analyses, $\xi = 2.78$ and $\phi = -1.07$ [4] and $\xi \simeq 0.4$ and $\phi = 3.14$ [5,6], are disfavoured with a $\chi^2$ of 68 (C.L.$\sim 10^{-4}$) and 49 (C.L. = 3%) respectively, for 32 $dof$.

## 2.3 $\eta'$ transition form factor

In this paper, we use a new technique to determine the $Q^2$ value of the untagged events. The Monte Carlo simulation demonstrates that $Q^2 = |\vec{p}_t(\pi^+\pi^-\gamma)|^2$ within the experimental resolution (Fig. 5). For the events of Group-II, the data are subdivided into three $Q^2$ intervals (Figs. 6a-c). In this Group, the background is higher because there is no efficient cut to remove events with additional undetected particles. However, the narrow $\eta'$ signal is still clearly seen above the background. The numbers of $\eta'$ events are obtained by fitting each distribution to a gaussian for the $\eta'$ signal, superimposed on a polynomial background. The results are summarised in Table 1.

For the tagged events, Group-III, the $\pi^+\pi^-\gamma$ mass spectrum is shown in Fig. 6d. A clear $\eta'$ signal is observed over a low background. These tagged events are subdivided into two $\mathrm{Q}^2$ intervals (Table 1).

The cross section is measured in each $Q^2$ interval using:

$$\Delta\sigma = \frac{\Delta N}{\mathcal{L} \cdot \varepsilon \cdot BR} \tag{9}$$

where $\Delta N$ is the measured number of $\eta'$ events, $\mathcal{L}$ is the total integrated $e^+e^-$ luminosity and $\varepsilon$ is the product of the detector acceptance and efficiency. The total integrated luminosity is 129 $\text{pb}^{-1}$ for untagged events and 100 $\text{pb}^{-1}$ for tagged events. The measured cross sections and the average $Q^2$ are also listed in Table 1. The average $Q^2$ values quoted take into account the $Q^2$ dependence of the spectrum within each interval. The systematic uncertainty on the selection efficiency is the same in all groups. The additional uncertainty from the background subtraction varies from 3% to 9% for the different $Q^2$ intervals.

The decrease of the cross section as a function of $Q^2$ is due to the two-photon luminosity function, the matrix element $\sqrt{X}$ and the resonance form factor. The effects of the luminosity function and of the matrix element are removed by generating events with a flat form factor $(F(Q^2)/F(0) = 1)$. The $\eta'$ transition form factor is then given by the ratio between the data and this Monte Carlo. The transition form factor is also corrected for the four momentum squared $k^2$ of the second photon. This effect is studied by generating events with different input $\Lambda$ values ($0.77 - 1.01$ GeV) in Eq. 3. The corrected results are given in Table 1 and in Fig. 7. The effect of collinear initial state radiation on the form factor is found to be negligible; it is less than 1% for Group-II untagged events and 3% for Group-III tagged events. The five high $Q^2$ points are fitted with the form factor parametrisation given in Eq. 3. In addition, the value at $Q^2 = 0$ is fixed to our measured value of $\Gamma_{\gamma\gamma} \cdot BR$. The value of the parameter $\Lambda$ obtained by the fit is:

$$\Lambda = 0.900 \pm 0.046 \text{ (stat.)} \pm 0.022 \text{ (sys.) GeV} \qquad \chi^2/dof = 0.7/4 \text{ (C.L.} = 95\%) \ .$$

The fit result is shown in Fig. 7a. The systematic error is due to the point-to-point systematic error of each cross section point (1.6%) and to the uncertainty of the two-photon width (1.9%). The value of $\Lambda$ would be 11% lower if the virtuality of the second photon were to be neglected. The effect of collinear initial state radiation on the fitted value of $\Lambda$ is smaller than 1%. The parameter $\Lambda$ is related to the interaction size of the $\eta'$: $\langle r^2 \rangle = 6/\Lambda^2$. From our data we obtain $\langle r^2 \rangle = 0.286 \pm 0.032$ fm$^2$. Our measurement compares well with previous published results [2].

For the pseudoscalar mesons $\pi^0$, $\eta$ and $\eta'$, there exist several models which describe the transition form factor. The Vector Dominance Model (VDM) relates $\Lambda$ to the masses of the vector mesons $\rho, \omega$ and $\phi$. Its prediction, $\Lambda = 0.83$ GeV [3], for a weighted average of the vector meson contributions, is shown in Fig. 7b as the dashed line. It is consistent with our data.

Recently QCD models have been developed to describe the $\pi^0$ form factor [16–19]. To provide predictions for the $\eta'$ form factor, the mixing of the singlet and octet components of the flavour SU(3) pseudoscalar nonet must be taken into account. In the chiral limit of vanishing quark masses the photon-pion transition form factor at $q^2 = k^2 = 0$ is fixed by the pion decay constant ($f_\pi = 130.7$ MeV [2)]). For $k^2 = 0$ and large $Q^2$, the QCD model of Brodsky and Lepage [17], expresses the form factor in terms of the asymptotic wave function of the quark inside the pion, $\Phi(x) = \sqrt{3/2} f_\pi x(1-x)$:

$$F_{\pi\gamma}(Q^2) = (4\pi\alpha) \cdot \frac{2}{\sqrt{3}Q^2} \int_0^1 dx \frac{\Phi(x)}{x(1-x)} \quad , \quad F_{\pi\gamma}(Q^2 \to \infty) = (4\pi\alpha) \cdot \frac{\sqrt{2} f_\pi}{Q^2} \ . \tag{10}$$

Here $x$ is the momentum fraction of the quark inside the pion. Brodsky and Lepage interpolate between the $Q^2 = 0$ and $Q^2 \to \infty$ limits with the pole form of Eq. 3 giving a parameter: $\Lambda_{\eta'} = 0.8 \times 2\pi f_\pi = 0.66$ GeV [3, 17]. This prediction is also shown in Fig. 7b. In their hard scattering approach, R. Jacob, P. Kroll and M. Raulfs [18] consider also the transverse degree of freedom for the $q\bar{q}$ wave function and include resummed gluonic corrections in a Sudakov factor. Their calculation reproduces our high $Q^2$ data better than the original Brodsky - Lepage model (Fig. 7b).

In order to cover the low and moderately high $Q^2$ region of the photon-meson transition form factor, V.V. Anisovich, D.I. Melikhov and V.A. Nikonov [19] introduce a $q\bar{q}$ distribution function at the $\gamma q\bar{q}$ vertex similar to the pion distribution function describing the $\pi q\bar{q}$ vertex; i.e. the photon is treated much like a vector meson. At large $Q^2$ the photon wave function contains the point-like $q\bar{q}$ coupling and the $O(\alpha_s)$ one gluon exchange diagrams. They also explore the possibility that the $\eta$ and the $\eta'$ contain an extra glueball component [20]. Their predictions are given in Fig. 7a for a variable admixture of gluonium content. Our measurement favours a low gluonium content. More precise calculations and more luminosity are needed to draw firmer conclusions.

[2)] One may note that with the definition of $f_\pi$ of Ref. [2, 17], this value would be lower by a factor of $1/\sqrt{2}$.

# 3 Conclusions

A high statistics sample of $e^+e^- \rightarrow e^+e^-\eta'$, $\eta' \rightarrow \pi^+\pi^-\gamma$ events has been collected with the L3 detector at LEP energies around 91 GeV. The channel is dominated by the decay $\eta' \rightarrow \rho\gamma$. We find no positive evidence for a box anomaly contribution in this decay mode. From the quasi-real two-photon interaction the $\eta'$ radiative width: $\Gamma_{\gamma\gamma}(\eta') = 4.17 \pm 0.10$ (stat.)$\pm 0.27$ (sys.) keV is measured. This value is the most precise obtained in a single experiment. It is consistent with the world average value and is comparable in precision.

The $\eta'$ transition form factor has been measured in the interval $0.01 \leq Q^2 \leq 10.0$ GeV$^2$. A fit to the data with a pole parametrisation gives a value $\Lambda = 0.900 \pm 0.046$ (stat.)$\pm 0.022$ (sys.) GeV, which corresponds to an interaction size $\langle r^2 \rangle = 0.286 \pm 0.032$ fm$^2$. The pole form is a good representation of the data. The Vector Dominance Model and recent non-perturbative QCD calculations are also consistent with the data.

# Acknowledgements

We express our gratitude to the CERN accelerator divisions for the excellent performance of the LEP machine. We acknowledge with appreciation the effort of all engineers, technicians and support staff who have participated in the construction and maintenance of this experiment. We wish to thank P. Kroll, V.V. Anisovich and V.A. Nikonov for their help with the theoretical predictions.

| Group | $Q^2$ interval | $\langle Q^2 \rangle$ | $\eta'$ events | $\varepsilon$ | $\Delta\sigma(e^+e^- \rightarrow e^+e^-\eta')$ | $(m^3_{\eta'}/64\pi)F^2(Q^2)$ |
|---|---|---|---|---|---|---|
| | (GeV$^2$) | (GeV$^2$) | | (%) | (pb) | (keV) |
| I | 0.0 – 0.01 | 0.0 | 2123 $\pm$ 53 | 2.8 | 1924 $\pm$ 48 $\pm$ 19 | 4.17 $\pm$ 0.10 $\pm$ 0.04 |
| II | 0.01 – 0.15 | 0.06 | 726 $\pm$ 47 | 3.7 | 510 $\pm$ 33 $\pm$ 15 | 3.51 $\pm$ 0.23 $\pm$ 0.11 |
| | 0.15 – 0.30 | 0.23 | 123 $\pm$ 18 | 2.9 | 109 $\pm$ 16 $\pm$ 4 | 2.78 $\pm$ 0.41 $\pm$ 0.11 |
| | 0.30 – 0.90 | 0.53 | 58 $\pm$ 11 | 1.7 | 88 $\pm$ 17 $\pm$ 5 | 1.50 $\pm$ 0.29 $\pm$ 0.09 |
| III | 1.50 – 2.50 | 1.90 | 17 $\pm$ 5 | 5.3 | 10.4 $\pm$ 3.3 $\pm$ 0.9 | 0.38 $\pm$ 0.12 $\pm$ 0.03 |
| | 2.50 – 10.0 | 4.14 | 19 $\pm$ 6 | 10.3 | 6.1 $\pm$ 1.8 $\pm$ 0.5 | 0.11 $\pm$ 0.03 $\pm$ 0.01 |

Table 1: Number of $\eta'$ events and cross sections $\Delta\sigma(e^+e^- \rightarrow e^+e^-\eta')$ as a function of $Q^2$. The total acceptance and efficiency $\varepsilon$ are given. In the last column the electromagnetic transition form factor, corrected for the virtuality of the second photon, is calculated for each $\langle Q^2 \rangle$. The first error is statistical and the second is point-to-point systematic. In addition, there is an overall scale error on $\Delta\sigma$ and on the form factor of 6.5% (4.3% from the branching ratio of $\eta' \rightarrow \pi^+\pi^-\gamma$ and 4.9% from the selection cuts).

# References


[1] Mark II Coll., G. Abrams et al., Phys. Rev. Lett. 43 (1979) 477;
CELLO Coll., H.J. Behrend et al., Phys. Lett. B 114 (1982) 378; B 125 (1983) 518;
JADE Coll., W. Bartel et al., Phys. Lett. B 113 (1982) 190;
PLUTO Coll., Ch. Berger et al., Phys. Lett. 142 (1984) 125;
TASSO Coll., M. Althoff et al., Phys. Lett. B 147 (1984) 487;
ARGUS Coll., H. Alberecht etal., Phys. Lett. B 199 (1987) 457;
TPC-2$\gamma$ Coll., H. Aihara et al. , Phys. Rev. D 35 (1987) 2650;
TPC-2$\gamma$ Coll., H. Aihara et al., Phys. Rev. D 38 (1988) 1;
Crystal Ball Coll., D.A. Williams et al., Phys. Rev. D 38 (1988) 1365;
Crystal Ball Coll., K. Karch et al, Z. Phys. C 54 (1992) 33;
ASP Coll., N.A. Roe et al., Phys. Rev. D 41 (1990) 17;
Mark II Coll., F. Butler et al., Phys. Rev. D 42 (1990) 1368;
MD-1 Coll., S.E. Baru et al., Z. Phys. C 48 (1990) 581.

[2] TPC-2$\gamma$ Coll., H. Aihara et al., Phys. Rev. Lett. 64 (1990) 172;
CELLO Coll., H.J. Behrend et al , Z. Phys. C 49 (1991) 401.

[3] Ll. Ametler, J. Bijnens, A. Bramon, F. Cornet, Phys. Rev. D 45 (1992) 986 and references therein.

[4] S.I. Bityukov et al., Z. Phys. C 50 (1991) 451.

[5] M. Benayoun et al., Z. Phys. C 58 (1993) 31.

[6] Crystal Barrel Coll., A. Abele et al., Phys. Lett. B 402 (1997) 195.

[7] J.D. Jackson, Nuovo Cimento 34 (1964) 1644.

[8] Review of Particle Physics, Phys. Rev. D 54 (1996) 1.

[9] EGPC generator; F.L. Linde, PhD thesis, Rijksuniversiteit te Leiden (1988).

[10] V.M. Budnev et al., Phys. Rep. 15 (1975) 181.

[11] R. Brun et al., GEANT 3.15 preprint CERN DD/EE/84-1 (Revised 1987).

[12] H. Fesefeldt, RWTH Aachen report PITHA 85/2 (1985).

[13] L3 Coll., B. Adeva et al., Nucl. Inst. Meth. A289 (1990) 35;
J.A. Bakken et al., Nucl. Inst. Meth. A275 (1989) 81;
O. Adriani et al., Nucl. Inst. Meth. A302 (1991) 53;
B. Adeva et al., Nucl. Inst. Meth. A323 (1992) 109;
K. Deiters et al., Nucl. Inst. Meth. A323 (1992) 162;
M. Chemarin et al., Nucl. Inst. Meth. A349 (1994) 345;
M. Acciarri et al., Nucl. Inst. Meth. A351 (1994) 300;
G. Basti et al., Nucl. Inst. Meth. A374 (1996) 293;
A. Adam et al., Nucl. Inst. Meth. A383 (1996) 342.

[14] L3 Coll., M. Acciarri et al., CERN-PPE/97-68, submitted to Phys. Lett. B.

[15] E. Klempt, B.C. Metsch, C.R. Münz and H.R. Petry, Phys. Lett. B 361 (1995) 160;
C.R. Münz, Nucl. Phys. A 609 (1996) 364.

[16] S. Ong, Phys. Rev. D 52 (1995) 3111;
M.R. Frank, K.L. Mitchell, C.D. Roberts and P.C. Tandy, Phys. Lett. B 359 (1995) 17;
D. Kekez and D. Klabucar, Phys. Lett. B 387 (1996) 14;
F.G. Cao, T. Hung and B.Q. Ma, Phys. Rev. D 53 (1996) 6582;
A.V. Radyushkin and R. Ruskov, Phys. Lett. B 374 (1996) 173.

[17] S.J. Brodsky and G. P. Lepage, Phys. Rev. D 24 (1981) 1808.

[18] R. Jacob, P. Kroll and M. Raulfs, J. Phys. G 22 (1996) 45.

[19] V.V. Anisovich, D.I. Melikhov and V.A. Nikonov, Phys. Rev. D 55 (1997) 2918.

[20] V.V. Anisovich, D.V. Bugg, D.I. Melikhov and V.A. Nikonov, hep-ph/9702383, to be published in Phys. Lett. B.

# The L3 Collaboration:

M.Acciarri,[28] O.Adriani,[17] M.Aguilar-Benitez,[27] S.Ahlen,[11] J.Alcaraz,[27] G.Alemanni,[23] J.Allaby,[18] A.Aloisio,[30] G.Alverson,[12] M.G.Alviggi,[30] G.Ambrosi,[20] H.Anderhub,[50] V.P.Andreev,[39] T.Angelescu,[13] F.Anselmo,[9] A.Arefiev,[29] T.Azemoon,[3] T.Aziz,[10] P.Bagnaia,[38] L.Baksay,[45] R.C.Ball,[3] S.Banerjee,[10] Sw.Banerjee,[10] K.Banicz,[47] A.Barczyk,[50,48] R.Barillère,[18] L.Barone,[38] P.Bartalini,[35] A.Baschirotto,[28] M.Basile,[9] R.Battiston,[35] A.Bay,[23] F.Becattini,[17] U.Becker,[16] F.Behner,[50] J.Berdugo,[27] P.Berges,[16] B.Bertucci,[35] B.L.Betev,[50] S.Bhattacharya,[10] M.Biasini,[18] A.Biland,[50] G.M.Bilei[35] J.J.Blaising,[4] S.C.Blyth,[36] G.J.Bobbink,[2] R.Bock,[1] A.Böhm,[1] L.Boldizsar,[14] B.Borgia,[38] D.Bourilkov,[50] M.Bourquin,[20] D.Boutigny,[4] S.Braccini,[20] J.G.Branson,[41] V.Brigljevic,[50] I.C.Brock,[36] A.Buffini,[17] A.Buijs,[46] J.D.Burger,[16] W.J.Burger,[20] J.Busenitz,[45] X.D.Cai,[16] M.Campanelli,[50] M.Capell,[16] G.Cara Romeo,[9] G.Carlino,[30] A.M.Cartacci,[17] J.Casaus,[27] G.Castellini,[17] F.Cavallari,[38] N.Cavallo,[30] C.Cecchi,[20] M.Cerrada,[27] F.Cesaroni,[24] M.Chamizo,[27] Y.H.Chang,[52] U.K.Chaturvedi,[19] S.V.Chekanov,[32] M.Chemarin,[26] A.Chen,[52] G.Chen,[7] G.M.Chen,[7] H.F.Chen,[21] H.S.Chen,[7] M.Chen,[16] G.Chiefari,[30] C.Y.Chien,[5] L.Cifarelli,[40] F.Cindolo,[9] C.Civinini,[17] I.Clare,[16] R.Clare,[16] H.O.Cohn,[33] G.Coignet,[4] A.P.Colijn,[2] N.Colino,[27] V.Commichau,[1] S.Costantini,[8] F.Cotorobai,[13] B.de la Cruz,[27] A.Csilling,[14] T.S.Dai,[16] R.D'Alessandro,[17] R.de Asmundis,[30] A.Degré,[4] K.Deiters,[48] P.Denes,[37] F.DeNotaristefani,[38] D.DiBitonto,[45] M.Diemoz,[38] D.van Dierendonck,[2] F.Di Lodovico,[50] C.Dionisi,[38] M.Dittmar,[50] A.Dominguez,[41] A.Doria,[30] M.T.Dova,[19,♯] E.Drago,[30] D.Duchesneau,[4] P.Duinker,[2] I.Duran,[42] S.Dutta,[10] S.Easo,[35] Yu.Efremenko,[33] H.El Mamouni,[26] A.Engler,[36] F.J.Eppling,[16] F.C.Erné,[2] J.P.Ernenwein,[26] P.Extermann,[20] M.Fabre,[48] R.Faccini,[38] S.Falciano,[38] A.Favara,[17] J.Fay,[26] O.Fedin,[39] M.Felcini,[50] B.Fenyi,[45] T.Ferguson,[36] F.Ferroni,[38] H.Fesefeldt,[1] E.Fiandrini,[35] J.H.Field,[20] F.Filthaut,[36] P.H.Fisher,[16] I.Fisk,[41] G.Forconi,[16] L.Fredj,[20] K.Freudenreich,[50] C.Furetta,[28] Yu.Galaktionov,[29,16] S.N.Ganguli,[10] P.Garcia-Abia,[49] S.S.Gau,[12] S.Gentile,[38] J.Gerald,[5] N.Gheordanescu,[13] S.Giagu,[38] S.Goldfarb,[23] J.Goldstein,[11] Z.F.Gong,[21] A.Gougas,[5] G.Gratta,[34] M.W.Gruenewald,[8] V.K.Gupta,[37] A.Gurtu,[10] L.J.Gutay,[47] B.Hartmann,[1] A.Hasan,[31] D.Hatzifotiadou,[9] T.Hebbeker,[8] A.Hervé,[18] W.C.van Hoek,[32] H.Hofer,[50] S.J.Hong,[44] H.Hoorani,[36] S.R.Hou,[52] G.Hu,[5] V.Innocente,[18] K.Jenkes,[1] B.N.Jin,[7] L.W.Jones,[3] P.de Jong,[18] I.Josa-Mutuberria,[27] A.Kasser,[23] R.A.Khan,[19] D.Kamrad,[49] Yu.Kamyshkov,[33] J.S.Kapustinsky,[25] Y.Karyotakis,[4] M.Kaur,[19,◇] M.N.Kienzle-Focacci,[20] D.Kim,[38] D.H.Kim,[44] J.K.Kim,[44] S.C.Kim,[44] Y.G.Kim,[44] W.W.Kinnison,[25] A.Kirkby,[34] D.Kirkby,[34] J.Kirkby,[18] D.Kiss,[14] W.Kittel,[32] A.Klimentov,[16,29] A.C.König,[32] A.Kopp,[49] I.Korolko,[29] V.Koutsenko,[16,29] R.W.Kraemer,[36] W.Krenz,[1] A.Kunin,[16,29] P.Lacentre,[49,♮,♯] P.Ladron de Guevara,[27] G.Landi,[17] C.Lapoint,[16] K.Lassila-Perini,[50] P.Laurikainen,[22] M.Lebeau,[18] A.Lebedev,[16] P.Lebrun,[26] P.Lecomte,[50] P.Lecoq,[18] P.Le Coultre,[50] H.J.Lee,[8] C.Leggett,[3] J.M.Le Goff,[18] R.Leiste,[49] E.Leonardi,[38] P.Levtchenko,[39] C.Li,[21] C.H.Lin,[52] W.T.Lin,[52] F.L.Linde,[2,18] L.Lista,[30] Z.A.Liu,[7] W.Lohmann,[49] E.Longo,[38] W.Lu,[34] Y.S.Lu,[7] K.Lübelsmeyer,[1] C.Luci,[38] D.Luckey,[16] L.Luminari,[38] W.Lustermann,[48] W.G.Ma,[21] M.Maity,[10] G.Majumder,[10] L.Malgeri,[38] A.Malinin,[29] C.Maña,[27] D.Mangeol,[32] S.Mangla,[10] P.Marchesini,[50] A.Marin,[11] J.P.Martin,[26] F.Marzano,[38] G.G.G.Massaro,[2] D.McNally,[18] S.Mele,[30] L.Merola,[30] M.Meschini,[17] W.J.Metzger,[32] M.von der Mey,[1] Y.Mi,[23] A.Mihul,[13] A.J.W.van Mil,[32] H.Milcent,[18] G.Mirabelli,[38] J.Mnich,[18] P.Molnar,[8] B.Monteleoni,[17] R.Moore,[3] S.Morganti,[38] T.Moulik,[10] R.Mount,[34] S.Müller,[1] F.Muheim,[20] A.J.M.Muijs,[2] S.Nahn,[16] M.Napolitano,[30] F.Nessi-Tedaldi,[50] H.Newman,[34] T.Niessen,[1] A.Nippe,[1] A.Nisati,[38] H.Nowak,[49] Y.D.Oh,[44] H.Opitz,[1] G.Organtini,[38] R.Ostonen,[22] C.Palomares,[27] D.Pandoulas,[1] S.Paoletti,[38] P.Paolucci,[30] H.K.Park,[36] I.H.Park,[44] G.Pascale,[38] G.Passaleva,[18] S.Patricelli,[30] T.Paul,[12] M.Pauluzzi,[35] C.Paus,[18] F.Pauss,[50] D.Peach,[18] Y.J.Pei,[1] S.Pensotti,[28] D.Perret-Gallix,[4] B.Petersen,[32] S.Petrak,[8] A.Pevsner,[5] D.Piccolo,[30] M.Pieri,[17] P.A.Piroué,[37] E.Pistolesi,[28] V.Plyaskin,[29] M.Pohl,[50] V.Pojidaev,[29,17] H.Postema,[16] N.Produit,[20] D.Prokofiev,[39] G.Rahal-Callot,[50] N.Raja,[10] P.G.Rancoita,[28] M.Rattaggi,[28] G.Raven,[41] P.Razis,[31] K.Read,[33] D.Ren,[50] M.Rescigno,[38] S.Reucroft,[12] T.van Rhee,[46] S.Riemann,[49] K.Riles,[3] O.Rind,[3] R.Rizzo,[28] A.Robohm,[50] J.Rodin,[16] B.P.Roe,[3] L.Romero,[27] S.Rosier-Lees,[4] Ph.Rosselet,[23] W.van Rossum,[46] S.Roth,[1] J.A.Rubio,[18] D.Ruschmeier,[8] H.Rykaczewski,[50] J.Salicio,[18] E.Sanchez,[27] M.P.Sanders,[32] M.E.Sarakinos,[22] S.Sarkar,[10] M.Sassowsky,[1] G.Sauvage,[4] C.Schäfer,[1] V.Schegelsky,[39] S.Schmidt-Kaerst,[1] D.Schmitz,[1] P.Schmitz,[1] M.Schneegans,[4] N.Scholz,[50] H.Schopper,[51] D.J.Schotanus,[32] J.Schwenke,[1] G.Schwering,[1] C.Sciacca,[30] D.Sciarrino,[20] L.Servoli,[35] S.Shevchenko,[34] N.Shivarov,[43] V.Shoutko,[29] J.Shukla,[25] E.Shumilov,[29] A.Shvorob,[34] T.Siedenburg,[1] D.Son,[44] V.Soulimov,[30] B.Smith,[16] P.Spillantini,[17] M.Steuer,[16] D.P.Stickland,[37] H.Stone,[37] B.Stoyanov,[43] A.Straessner,[1] K.Strauch,[15] K.Sudhakar,[10] G.Sultanov,[19] L.Z.Sun,[21] G.F.Susinno,[20] H.Suter,[50] J.D.Swain,[19] X.W.Tang,[7] L.Tauscher,[6] L.Taylor,[12] Samuel C.C.Ting,[16] S.M.Ting,[16] M.Tonutti,[1] S.C.Tonwar,[10] J.Tóth,[14] C.Tully,[37] H.Tuchscherer,[45] K.L.Tung,[7] Y.Uchida,[16] J.Ulbricht,[50] U.Uwer,[18] E.Valente,[38] R.T.Van de Walle,[32] G.Vesztergombi,[14] I.Vetlitsky,[29] G.Viertel,[50] M.Vivargent,[4] R.Völkert,[49] H.Vogel,[36] H.Vogt,[49] I.Vorobiev,[18,29] A.A.Vorobyov,[39] A.Vorvolakos,[31] M.Wadhwa,[6] W.Wallraff,[1] J.C.Wang,[16] X.L.Wang,[21] Z.M.Wang,[21] A.Weber,[1] F.Wittgenstein,[18] S.X.Wu,[19] S.Wynhoff,[1] J.Xu,[11] Z.Z.Xu,[21] B.Z.Yang,[21] C.G.Yang,[7] X.Y.Yao,[7] J.B.Ye,[21] S.C.Yeh,[52] J.M.You,[36] An.Zalite,[39] Yu.Zalite,[39] P.Zemp,[50] Y.Zeng,[1] Z.Zhang,[7] Z.P.Zhang,[21] B.Zhou,[11] Y.Zhou,[3] G.Y.Zhu,[7] R.Y.Zhu,[34] A.Zichichi,[9,18,19] F.Ziegler.[49]

1 I. Physikalisches Institut, RWTH, D-52056 Aachen, FRG[§]
III. Physikalisches Institut, RWTH, D-52056 Aachen, FRG[§]
2 National Institute for High Energy Physics, NIKHEF, and University of Amsterdam, NL-1009 DB Amsterdam, The Netherlands
3 University of Michigan, Ann Arbor, MI 48109, USA
4 Laboratoire d'Annecy-le-Vieux de Physique des Particules, LAPP,IN2P3-CNRS, BP 110, F-74941 Annecy-le-Vieux CEDEX, France
5 Johns Hopkins University, Baltimore, MD 21218, USA
6 Institute of Physics, University of Basel, CH-4056 Basel, Switzerland
7 Institute of High Energy Physics, IHEP, 100039 Beijing, China[△]
8 Humboldt University, D-10099 Berlin, FRG[§]
9 University of Bologna and INFN-Sezione di Bologna, I-40126 Bologna, Italy
10 Tata Institute of Fundamental Research, Bombay 400 005, India
11 Boston University, Boston, MA 02215, USA
12 Northeastern University, Boston, MA 02115, USA
13 Institute of Atomic Physics and University of Bucharest, R-76900 Bucharest, Romania
14 Central Research Institute for Physics of the Hungarian Academy of Sciences, H-1525 Budapest 114, Hungary[‡]
15 Harvard University, Cambridge, MA 02139, USA
16 Massachusetts Institute of Technology, Cambridge, MA 02139, USA
17 INFN Sezione di Firenze and University of Florence, I-50125 Florence, Italy
18 European Laboratory for Particle Physics, CERN, CH-1211 Geneva 23, Switzerland
19 World Laboratory, FBLJA Project, CH-1211 Geneva 23, Switzerland
20 University of Geneva, CH-1211 Geneva 4, Switzerland
21 Chinese University of Science and Technology, USTC, Hefei, Anhui 230 029, China[△]
22 SEFT, Research Institute for High Energy Physics, P.O. Box 9, SF-00014 Helsinki, Finland
23 University of Lausanne, CH-1015 Lausanne, Switzerland
24 INFN-Sezione di Lecce and Universitá Degli Studi di Lecce, I-73100 Lecce, Italy
25 Los Alamos National Laboratory, Los Alamos, NM 87544, USA
26 Institut de Physique Nucléaire de Lyon, IN2P3-CNRS,Université Claude Bernard, F-69622 Villeurbanne, France
27 Centro de Investigaciones Energeticas, Medioambientales y Tecnologicas, CIEMAT, E-28040 Madrid, Spain♭
28 INFN-Sezione di Milano, I-20133 Milan, Italy
29 Institute of Theoretical and Experimental Physics, ITEP, Moscow, Russia
30 INFN-Sezione di Napoli and University of Naples, I-80125 Naples, Italy
31 Department of Natural Sciences, University of Cyprus, Nicosia, Cyprus
32 University of Nijmegen and NIKHEF, NL-6525 ED Nijmegen, The Netherlands
33 Oak Ridge National Laboratory, Oak Ridge, TN 37831, USA
34 California Institute of Technology, Pasadena, CA 91125, USA
35 INFN-Sezione di Perugia and Universitá Degli Studi di Perugia, I-06100 Perugia, Italy
36 Carnegie Mellon University, Pittsburgh, PA 15213, USA
37 Princeton University, Princeton, NJ 08544, USA
38 INFN-Sezione di Roma and University of Rome, "La Sapienza", I-00185 Rome, Italy
39 Nuclear Physics Institute, St. Petersburg, Russia
40 University and INFN, Salerno, I-84100 Salerno, Italy
41 University of California, San Diego, CA 92093, USA
42 Dept. de Fisica de Particulas Elementales, Univ. de Santiago, E-15706 Santiago de Compostela, Spain
43 Bulgarian Academy of Sciences, Central Lab. of Mechatronics and Instrumentation, BU-1113 Sofia, Bulgaria
44 Center for High Energy Physics, Korea Adv. Inst. of Sciences and Technology, 305-701 Taejon, Republic of Korea
45 University of Alabama, Tuscaloosa, AL 35486, USA
46 Utrecht University and NIKHEF, NL-3584 CB Utrecht, The Netherlands
47 Purdue University, West Lafayette, IN 47907, USA
48 Paul Scherrer Institut, PSI, CH-5232 Villigen, Switzerland
49 DESY-Institut für Hochenergiephysik, D-15738 Zeuthen, FRG
50 Eidgenössische Technische Hochschule, ETH Zürich, CH-8093 Zürich, Switzerland
51 University of Hamburg, D-22761 Hamburg, FRG
52 High Energy Physics Group, Taiwan, China
§ Supported by the German Bundesministerium für Bildung, Wissenschaft, Forschung und Technologie
‡ Supported by the Hungarian OTKA fund under contract numbers T14459 and T24011.
♭ Supported also by the Comisión Interministerial de Ciencia y Technología
♯ Also supported by CONICET and Universidad Nacional de La Plata, CC 67, 1900 La Plata, Argentina
♮ Supported by Deutscher Akademischer Austauschdienst.
◇ Also supported by Panjab University, Chandigarh-160014, India
△ Supported by the National Natural Science Foundation of China.

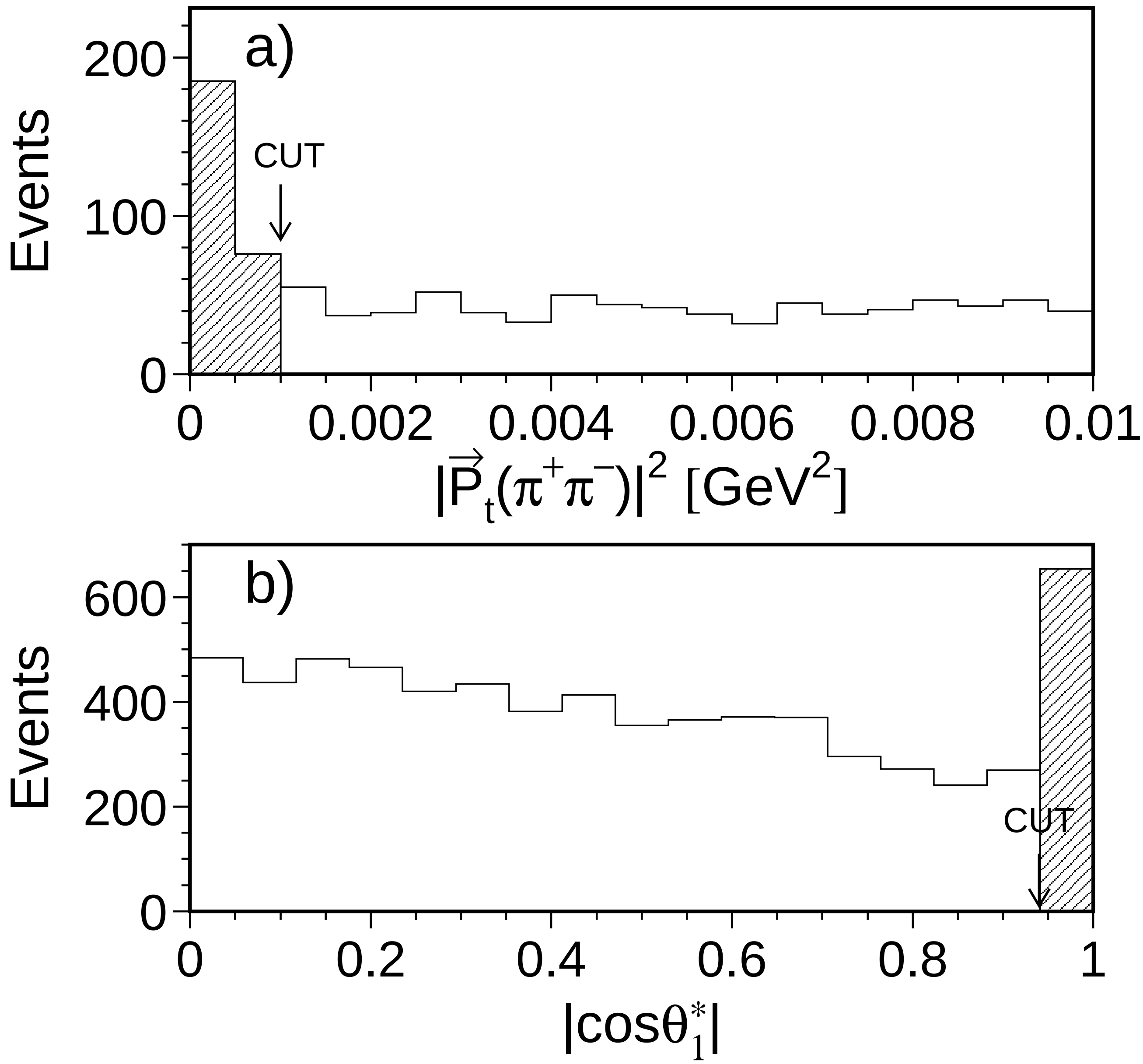


Figure 1: a) $|\vec{p}_t(\pi^+\pi^-)|^2$ spectrum and b) $|\cos\theta_1^*|$ distribution for the selection of $\pi^+\pi^-\gamma$ events. All cuts are applied except those indicated in the plots. Events excluded by the cuts are represented by the shaded area.

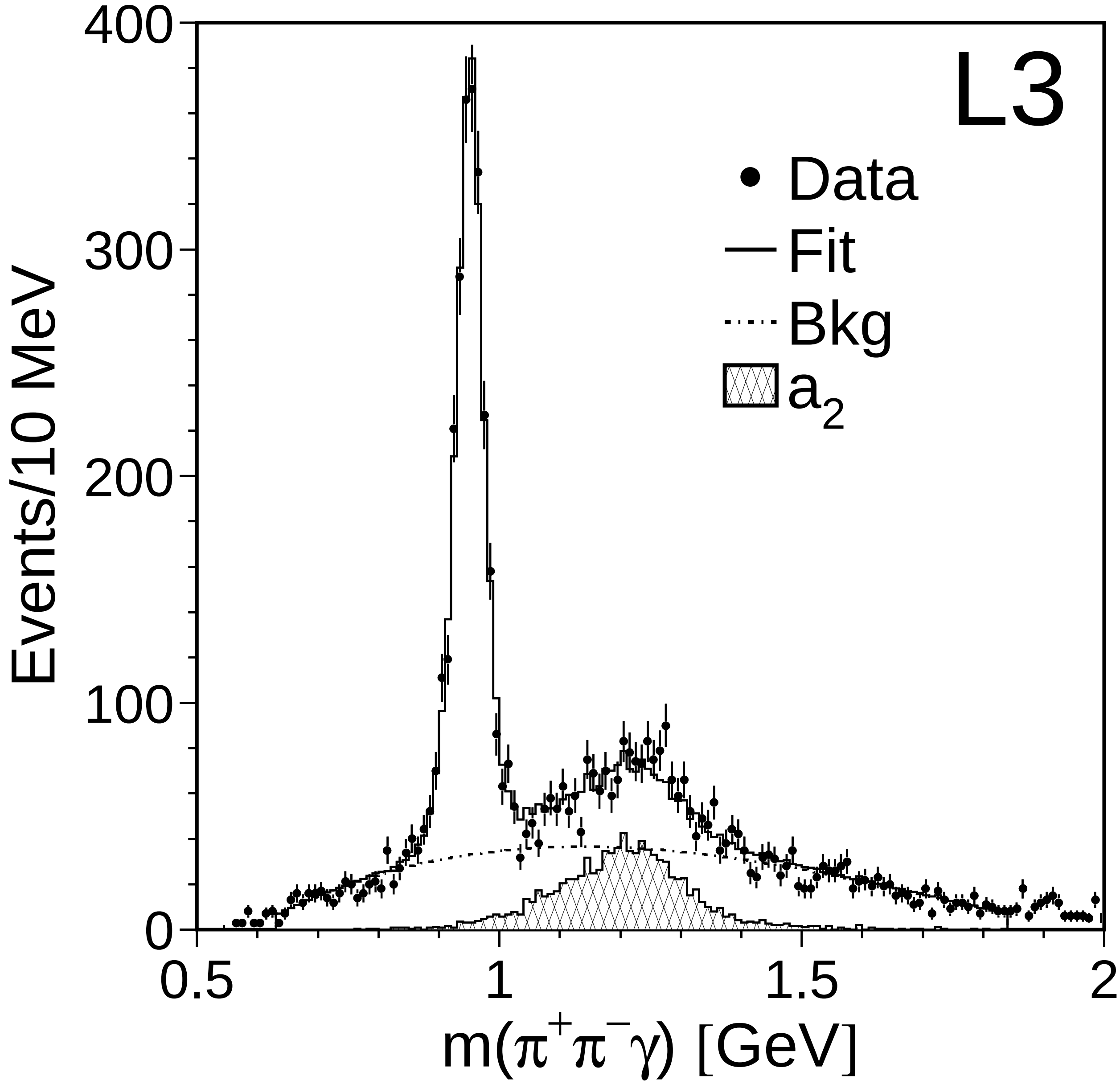


Figure 2: The reconstructed $\pi^+\pi^-\gamma$ mass spectrum for events with $Q^2 < 0.01$ GeV$^2$. The histogram is the result of the fit described in the text. The shaded area is the $a_2$ contribution and the dashed-dotted line is the fitted third order polynomial background.

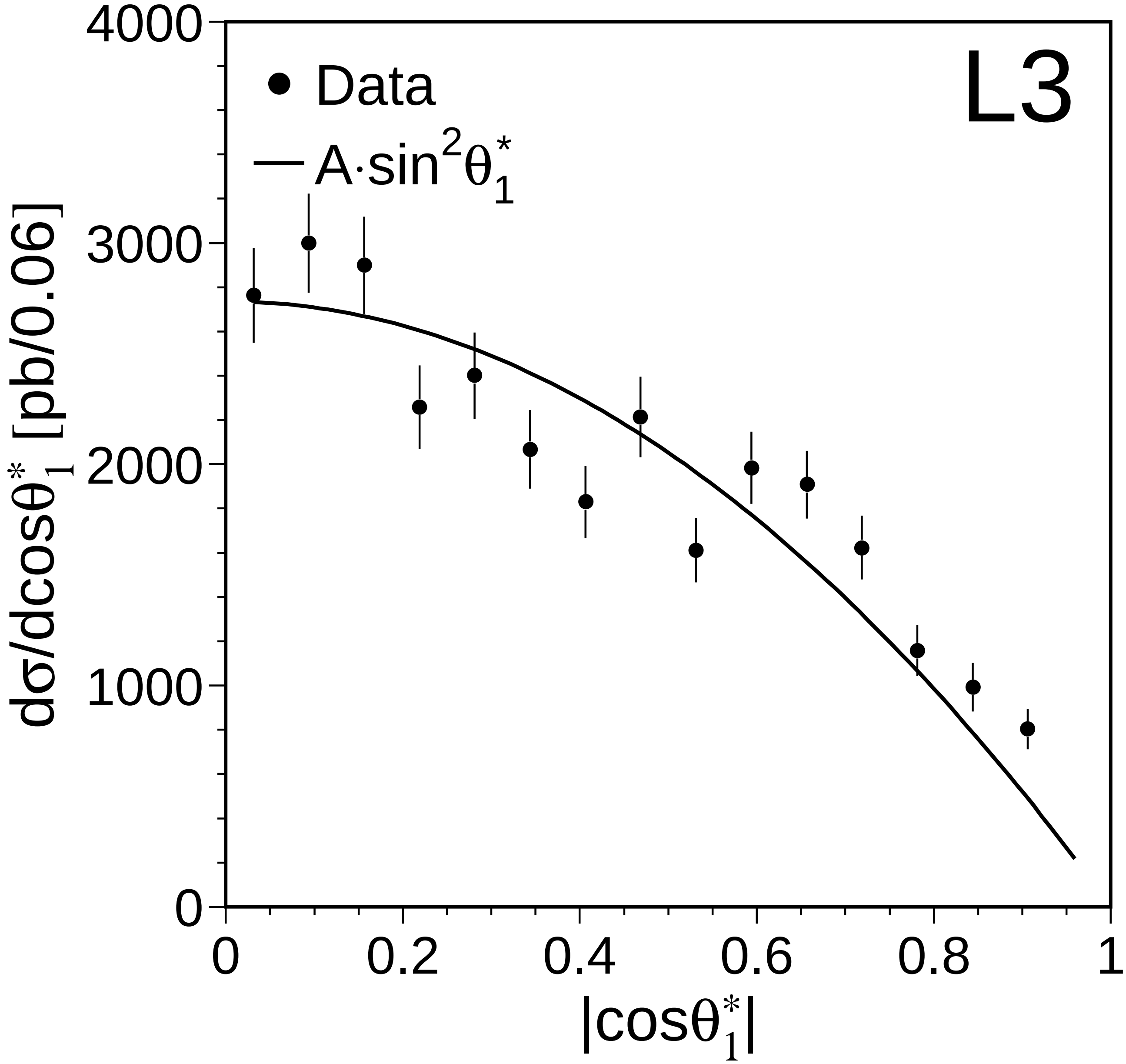


Figure 3: Background subtracted and efficiency corrected angular distribution of the $\pi^+$ in the $\rho$ helicity frame. The data are fitted to a $A\cdot \sin^2\theta_1^*$ distribution.

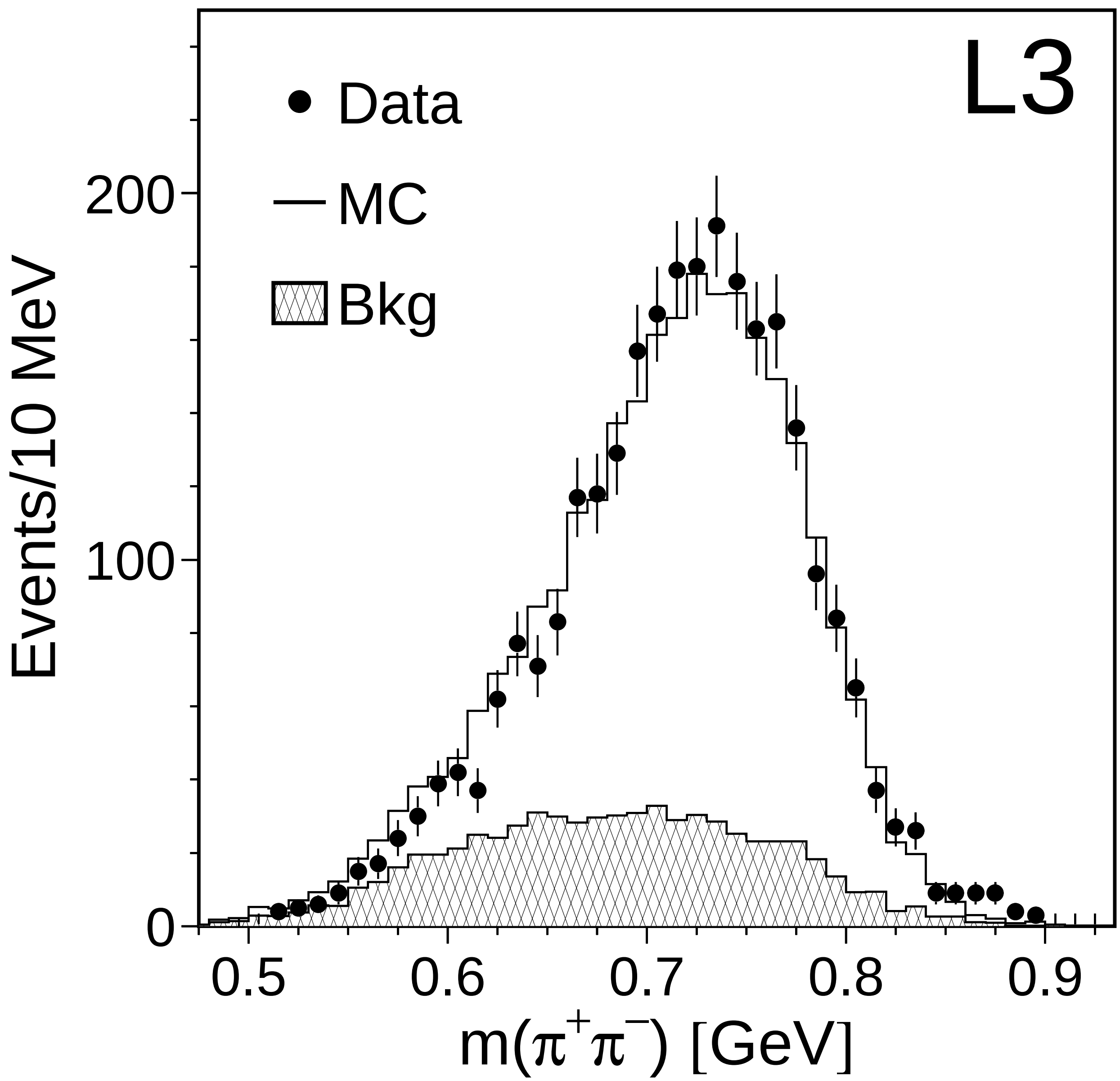


Figure 4: The uncorrected $\pi^+\pi^-$ effective mass distribution. The histogram is the prediction of the Monte Carlo which best fits the data ($m_\rho = 766$ MeV, $\Gamma_\rho = 150$ MeV and $\xi = 0$). The shaded area is the estimated background from $a_2$ and other inclusive processes simulated by assuming a three-body phase space distribution.

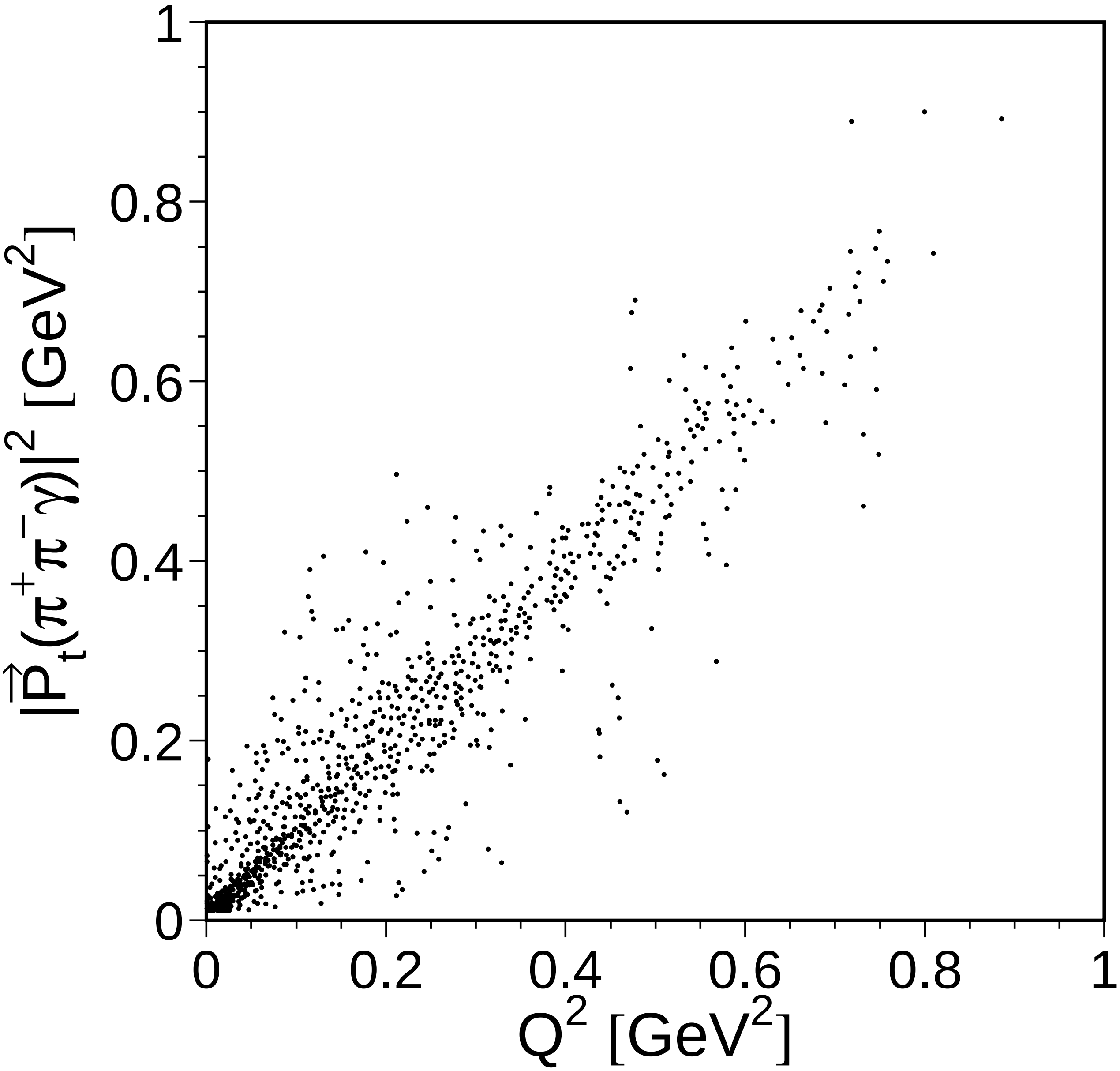


Figure 5: The transverse momentum squared of the reconstructed final state $\pi^+\pi^-\gamma$ versus the generated $Q^2$ (simulated events).

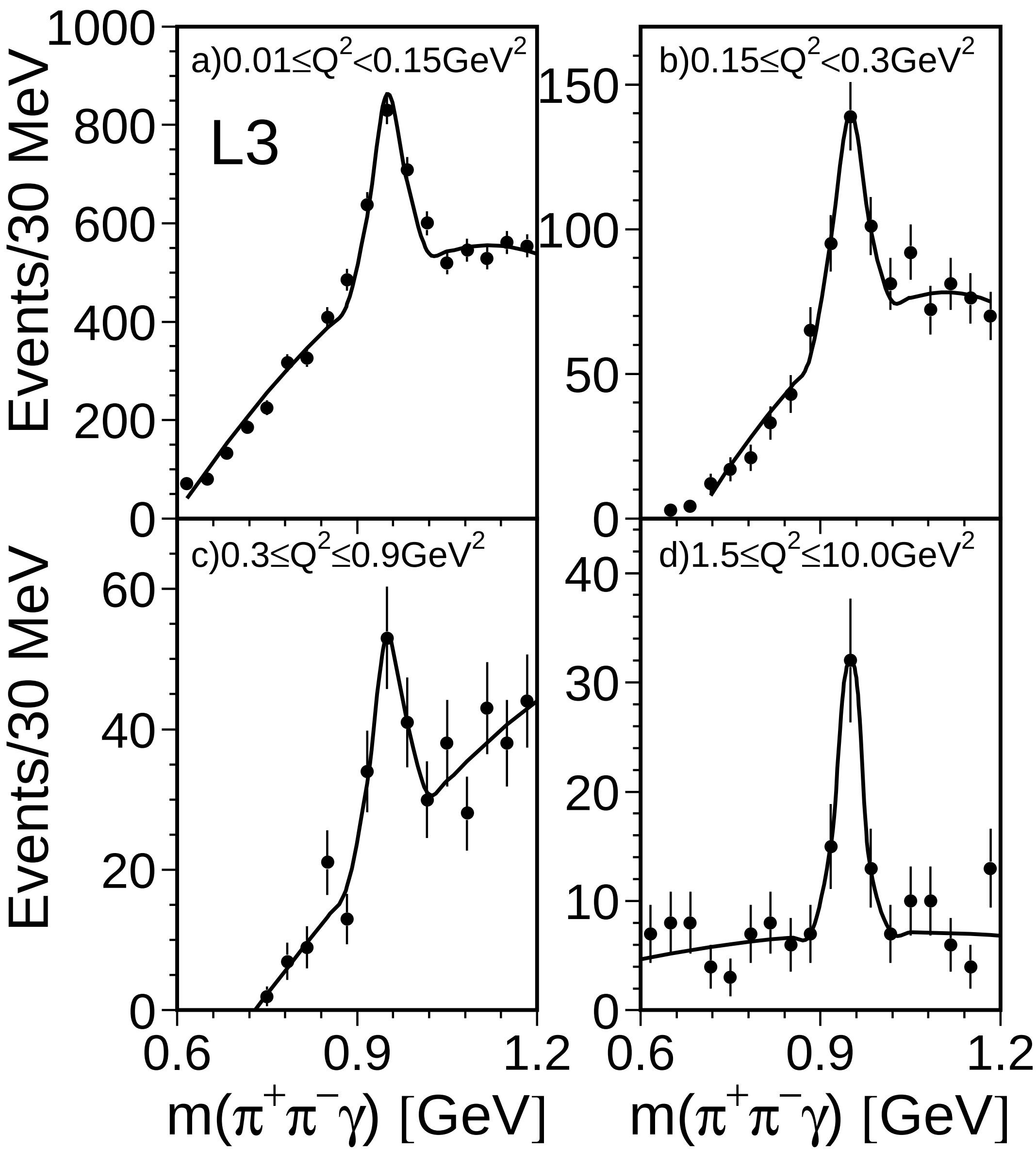


Figure 6: The reconstructed $\pi^+\pi^-\gamma$ mass spectrum for events with high $Q^2$, separated in four $Q^2$ intervals: a) $0.01 \leq Q^2 < 0.15$ GeV$^2$, b) $0.15 \leq Q^2 < 0.30$ GeV$^2$, c) $0.30 \leq Q^2 \leq 0.90$ GeV$^2$, d) Tagged events, $1.5 \leq Q^2 \leq 10.0$ GeV$^2$.

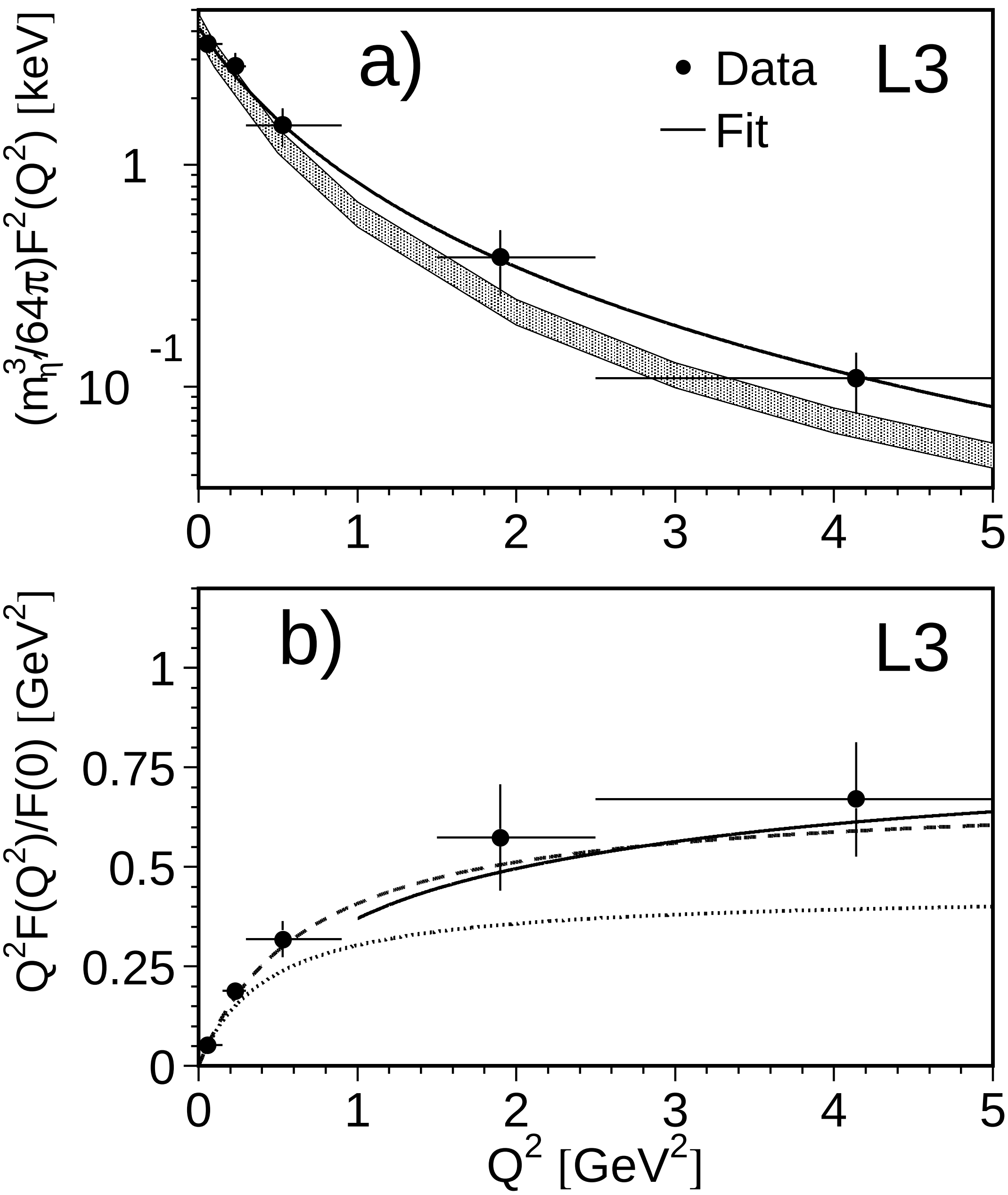


Figure 7: a) The quantity $(m_{\eta'}^3/64\pi)F^2(Q^2)$ measured at $\sqrt{s}$= 91 GeV. The errors shown are statistical and systematic added in quadrature. The solid line is the result of the pole fit to the data points described in the text. The predictions of Ref. [20] are indicated as a shaded area, ranging from no gluonium content (upper line) to 15% of gluonium content (lower line). b) The same data are given as $Q^2F(Q^2)$, normalised to $F(Q^2 = 0)$. The data are compared to QCD calculations [18] (continuous line), to VMD predictions [3] (dashed line) and to Ref. [17] (dotted) line.